# Molecular Mechanism of *Staphylococcus Xylosus* Resistance Against Tylosin and Florfenicol

**Xin liu**
guizhou zhongyiyao daxue: Guizhou University Of Traditional Chinese Medicine
**Shu li**
Shenzhen Institutes of Advanced Technology Chinese Academy of Sciences
**Wenqiang Cui**
Shenzhen Institutes of Advanced Technology Chinese Academy of Sciences
**Yonghui Zhou**
guizhou zhongyiyao daxue: Guizhou University Of Traditional Chinese Medicine
**Mo Chen**
Northeast Agricultural University
**Qianwei Qu**
Northeast Agricultural University
**Ruixiang Che**
Heilongjiang Bayi Nongken University: Heilongjiang Bayi Agricultural University
**Lu Li**
Northeast Agricultural University
**Horst Vogel**
Shenzhen Institutes of Advanced Technology Chinese Academy of Sciences
**Shuguang Yuan**
Shenzhen Institutes of Advanced Technology Chinese Academy of Sciences
**Yanhua Li** ( liyanhua@neau.edu.cn )
Northeast Agricultural University https://orcid.org/0000-0001-5578-3450

**Research Article**

**Keywords:** Antimicrobial resistance, Staphylococcus xylosus, cross-resistance evolution, ribosomal protein L22

**Posted Date:** June 24th, 2021

**DOI:** https://doi.org/10.21203/rs.3.rs-605410/v1

# Abstract

As a result of evolution, certain microbes develop resistance against antimicrobial treatment. The antimicrobial resistance (AMR) threatens the effective prevention and treatment of an ever-increasing range of severe infections caused by microbes such as bacteria, viruses, fungi and other parasites. The resistance of *Staphylococcus xylosus* (*S. xylosus*) against antibiotic treatment is one of the major causes of the world-wide antibiotic crisis and has remained to be well understood at the molecular level. In order to fill this gap, we investigated various mutations in the sequence of ribosomal proteins involved cross resistance. We discovered that for the mutant containing the insertion L22 97KRTSAIN98 the minimum inhibitory concentration against both tylosin and florfenicol changed dramatically. To understand this effect on a molecular basis and to further elucidate the role of cross resistance, we computationally constructed the 3D model of the large ribosomal subunit from *S. xylosus* as well as its complexes with both tylosin and florfenicol. Using all-atom molecular dynamics simulations, we found that unique structural changes in the β hairpin of L22 played a central role of this variant in the development of antibiotic resistance in *S. xylosus.* In addition, the regulation of protein network also played an essential role in the development of cross resistance in *S. xylosus*. Our work provides insightful views into the mechanism of *S. xylosus* resistance which could be useful for the development of the next generation of antibiotics.


# Introduction

Antibiotic resistance [1] occurs when bacteria or fungi develop the ability to defeat the drugs designed to kill them. As a result, germs will continue to grow and infections caused by antibiotic-resistant germs are difficult, sometimes even impossible, to treat. In most cases, antibiotic-resistant infections require extended healthcare which impose great social and economic burden. Antibiotic resistance affects people at any age and health condition making it one of the world's most urgent public health problems.

Each year in the U.S. about 2.8 million people are infected with antibiotic-resistant bacteria or fungi of whom 35,000 die. Worldwide about 700,000 people die each year due to drug-resistant diseases according to a report from World Health Organization (WHO) [2]. Figure 1 will soar to 10 million annually by 2050 according to WHO [3]. As crucial medicines become ineffective, without massive international investment and collaboration, future generations will face the disastrous impact of uncontrolled antimicrobial resistance. No one can completely avoid the risk of being affected by resistant infections. If antibiotics lose effectiveness, we lose the ability to treat serious infections and control public health.

*Staphylococcus xylosus* (*S.xylosus*) is a coagulase-negative, Gram-positive coccus that is widely distributed in the environment, as well as in the skin and mucosal surfaces of mammals (especially mice and humans) and birds [4, 5]. *S.xylosus* is also naturally present in raw meat and milk, and in addition, is used as starter culture for manufacturing sausage, fermented cheese and meat[6]. Although this strain is defined as an apparent nonpathogenic *Staphylococcus*, some strains unexpectedly appear involved in

bacterial infections in human and animal [7, 8.] Therefore, ever increasing attention is paid to the role *S. xylosus* plays in infectious diseases.

During the past few years, an increasing number of human infections have been associated with this species such as urinary tract, pancreatic, cardiac, ophthalmologic, dental, blood stream, erythema chest infections, nodosum as well as otogenic brain abscess, to mention a few [9–12]. Currently, *S.xylosus* has become the prevalent cause of mastitis in dairy herds in many countries including America, Finland, Canada, Sweden, Switzerland, Norway, and China [13–16] **(**Fig. 1**)**. The average proportion of mastitis due to *S.xylosus* increased year by year according to a nationwide survey [14, 17]. *S.xylosus* can also lead to other diseases in animals including dermatitis in gerbils and immune deficient mice, pulmonary and lymph node lesions in immune deficient mice, or transmural necrotizing cystitis and secondary peritonitis in a 4-month-old male Holstein calf [7, 18].

Nowadays, macrolides (tylosin), florfenicol, aminoglycosides (gentamicin and neomycin), and β-lactam antimicrobials (including penicillin and cephalosporins) are commonly used to treat mastitis **(Figure S1)**. Resistance to antibiotic used in mastitis are increasing[19, 20]. In several studies addressing evolution of resistance, one fearsome fact was observed, that bacteria developed cross-resistance against antimicrobial drugs to which they never have been exposed before [21]. Cross-resistance is a severe obstacle for designing effective drug therapies as it limits possible antibiotic options following an unsuccessful drug treatment. Surprisingly, evolution of cross-resistance in *S.xylosus* has not received much attention until very recently.

The ribosomal peptidyl transferase center (PTC) is critical for protein synthesis [22]. The peptidyl transferase reaction involves aminolysis by the α-amino group of the A-site aminoacyl-tRNA of the ester bond that links the nascent peptide to the 3 hydroxyl of the 3 terminal ribose of the P-site tRNA [23]. The PTC is densely packed and decorated with nucleotides of the central loop of domain V of 23S rRNA [23]. Many antibiotics that inhibit growth of microorganisms do so by binding to the PTC and inhibiting its activity. Notably, macrolides inhibit bacterial growth through interaction with PTC. Macrolides, such as erythromycin, azithromycin, carbomycin, tylosin, and others, bind at the upper portion of the ribosomal nascent peptide exit tunnel and target PTC [24]. Similarly, chloramphenicol, the first broad-spectrum antibiotic, inhibit protein synthesis by targeting the PTC of the bacterial ribosome. Because antibiotic binding should prevent the placement of aminoacyl-tRNA in the catalytic site, it is commonly assumed that these drugs are universal inhibitors of peptidyl transfer and should readily block the formation of new peptide bonds [25]. Accordingly, macrolides and chloramphenicol share the common mechanism of inhibition of PTC activity in bacteria and the cross-resistance mechanism of macrolides and chloramphenicol might be also related to PTC [24].

To better explore mechanism of antibiotic cross-resistance, we introduced site-selective mutations in the protein sequence, network regulations as well as computational modelling. We propose that in addition to the relationship of PTC and cross resistance, the regulation of protein network may be involved in mechanism of cross resistance. To elucidate the mechanism of resistance evolution of *S. xylosus* against

tylosin and florfenicol under selection pressure, we here further explore the before-mentioned resistant proteins. Furthermore, we investigate whether distinct mutations in ribosomal proteins are responsible for cross-resistance establishing mutant strains, using protein sequencing and computer simulations. Ultimately, quantitative PCR (qPCR) and computer simulations are applied to demonstrate that the resistant proteins are regulated by ribosomal proteins. Our present results demonstrate that mutations in ribosomal proteins are of central importance for the evolution of tylosin and florfenicol cross-resistance.

# Materials And Methods

### Plasmids, bacterial Strains, media, and growth conditions

Plasmids used in this study are listed in **Table S1**. *Staphylococcus xylosus* ATCC 700404 was purchased from the American Type Culture Collection (ATCC) and preserved in our lab. All tylosin-resistant *S. xylosus* were also kept in our lab. All mutants of *S. xylosus* were constructed in this study. The above strains **(Table S2)** are cultured in Tryptic Soy Broth (TSB) at 37°C.

### PCR amplification and DNA Sequencing of ribosome in *S. xylosus* and tylosin-resistant *S. xylosus*

Based on the genomes of *S. xylosus* and tylosin-resistant *S. xylosus* (tylosin 128μg/mL), the *rplC*, *rplD* and *rplV* fragments were amplified. All primers were listed in **Table S3**. According to the previous described method in our lab, the genomes of *S. xylosus* and tylosin-resistant *S. xylosus* were extracted. We choose the PrimeSTAR GXL DNA polymerase to amplify the fragments of *rplC*, *rplD* and *rplV*. Then, the PCR products were visualized by agarose gel electrophoresis. Furthermore, DNA sequences of PCR products were tested at Comate Bioscience company limited. Subsequently, the DNAMAN software was used to compare amino acid (nucleotide) sequence of *S. xylosus* with tylosin-resistant *S. xylosus*.

### Construction of the recombinant shuttle plasmids

The shuttle recombinant plasmids ($PBT_2$-*rplC*, $PBT_2$-*rplD* and $PBT_2$-*rplV*) were implemented according to a previous protocol in our lab with some modifications [26] **(Figure S2)**. The upstream and downstream fragment of *rplC*, *rplD* and *rplV* genes were amplified from the genomic DNA of *S. xylosus*. Meanwhile, the *gfp* gene and mutant fragments of *rplC*, *rplD* and *rplV* were received from plasmids, including gfp-T, mutant rplC-T, rplD-T and rplV-T. Then, as determinate order, the above PCR products were linked by overlap PCR and cloned to pClone007 Blunt Simple vector. The constructed plasmids were named based on mutant sites as pClone007-rplC, pClone007-rplD and pClone007-rplV. Next, the constructed plasmids were digested and cloned using the restriction sites of the *E.coli-Staphylococcus* shuttle vector pBT2, thus the recombinant shuttle plasmids PBT2-*rplC*, PBT2-*rplD* and PBT2-*rplV* were received. The above primers and restriction sites used in this section were listed in **Table S4**.

### Construction of the mutant *S. xylosus*

The mutant strains were created using a previously described protocol [27] with some modifications **(Figure S2)**. The above recombinant shuttle plasmids were introduced into *S. xylosus* by electroporation. The strains with recombinant shuttle plasmids were grown in TSB at 37 °C for 24 hours, then transferred to fresh medium at 42 °C for another 24 hours, which was identified as one passage. Based on the *gfp* gene, flow Cytometry (FC) was used to detect the mutant strains of 7, 9 and 11 passages. Meanwhile, the blank strains without recombinant shuttle plasmid served as control. Furthermore, the mutant strains screened by FC were identified by PCR amplification and sequences of mutant fragments **(Figure S3)**. Finally, the mutant strains were named as L3 (*rplC*) N135G, A137G, S142A and R162K mutant *S. xylosus*, L4 (*rplD*) S158N and A164E mutant *S.xylosus*, L22 (*rplV*) 97KRTSAIN98 insertion mutant *S. xylosus*.

## Evaluation of mutant *S. xylosus* susceptibility

Minimal inhibitory concentration (MIC) assays of tylosin and florfenicol to *S. xylosus* and mutant *S. xylosus* were done as previously reported [28]. Briefly, *S. xylosus* and mutant *strains* were grown overnight at 37 ℃. The overnight cultures were diluted in sterile physiological saline, which correspond to $1 \times 10^8$ colony-forming units/mL. Then, the cultures were diluted again with TSB to $1 \times 10^6$ colony-forming units/mL. Finally, 100 mL samples were added to the 96-well plate containing serial dilutions of tylosin in culture medium. Control bacterial and medium were cultivated in the absence of tylosin. The MIC was defined as the lowest concentration of inhibitor to visually inhibit growth. The above assays were repeated 3 times.

## MD simulation

We employed MD simulations for *S. xylosus* 23S rRNA, L22 and L22 97KRTSAIN98 insertion mutant to obtain reasonable corresponding three-dimensional structures and study the functional changes in the structure. All MD simulations were performed using GROMACS v2018 package [29]. All systems were solvated in a cubic water box with a 12 Å buffer distance between the solvent box wall and the nearest solute atoms and neutralized by addition of 150 mM $Na^+$ or $Cl^-$ ions. AMBER99SB-ILDN force field was assigned to the RNA, protein, and ions [30]. Water was modeled using the TIP3P water model. All structure models were first minimized to relax the solvent and optimize the system using steepest descent. Then, a short 100 ps NVT pre-equilibration simulation was performed whereby the heavy atoms of RNA or protein were positional restrained using a force constant of 200 kJ/(mol•nm). Finally, the production run, containing 23S rRNA and L22, were positional restrained in which to the backbone of ribose (C1’ atom), phosphate (P atom) and Cα atom a ositional force constant of 200 kJ/(mol•nm) was applied. L22 and L22 97KRTSAIN98 insertion mutant production runs were performed without any positional constraints. The temperature of simulations was controlled using the Nose-Hoover thermostat and the pressure was held at 1 bar using an isotropic coupling to the Parrinello-Rahman barostat. Long-range electrostatic interactions were calculated using the particle mesh Ewald method with a real-space cut off value of 1.2 nm. Nonbonded interactions were cut off at 1.2 nm.

## Docking

The docking of antibiotics to the receptor was performed using Glide [31]. Tylosin and florfenicol were produced in Schrodinger Maestro software. The LigPrep module in Schrodinger software was introduced for geometric optimization using OPLS_2005 force field. The receptor models were prepared in Schrodinger software under OPLS_2005 force field. Hydrogen atoms were added according to the physiological pH (7.5) with the PROPKA tool in Protein Preparation tool in Maestro to optimize the hydrogen bond network. Constrained energy minimizations were conducted on the full-atomic models. Cubic boxes centered on the tylosin and florfenicol mass center with a radius 12 Å for peptide exit tunnel and PTC of receptor.

## Investigation of resistant proteins in the evolution of tylosin-resistant *S. xylosus* at the mRNA level

Here, five proteins related to resistance were investigated at the mRNA level (16s rRNA was used as an internal control). Moreover, the primers of target genes are listed in **Table S5**. Total RNA of different levels of tylosin-resistant *S. xylosus* was extracted as specified by manufacturer, including tylosin (8 μg/mL, 32 μg/mL and 128 μg/mL). Next, equivalent amount of total DNA-free RNA from the last sample was reverse-transcribed using Prim-Script TM RT reagent kit with gDNA Eraser. Finally, the real time PCR program was performed for 40 cycles (95 ℃ for 15 s, 60 ℃ for 35 s) after initial 30 s incubation at 95 ℃. The assays were repeated 3 times.

## Investigation of resistant proteins in the evolution of tylosin-resistant *S. xylosus* at mRNA level

Here, five proteins related to resistance were investigated at the mRNA level (16s rRNA was used as an internal control). Moreover, the primers of target genes are listed in **Table S5**. Total RNA of different levels of tylosin-resistant *S. xylosus* was extracted as specified by the manufacturer, including tylosin (8 μg/mL, 32 μg/mL and 128 μg/mL). Next, equivalent amount of total DNA-free RNA from the last sample was reverse-transcribed using Prim-Script TM RT reagent kit with gDNA Eraser. Finally, the real time PCR program was performed for 40 cycles (95 ℃ for 15 s, 60 ℃ for 35 s) after initial 30 s incubation at 95 ℃. The assays were repeated 3 times.

## Investigation of resistant proteins in mutant *S. xylosus* at mRNA level

Here, five proteins related to resistance were investigated at mRNA level. 16S rRNA was used as an internal control. The list of primers is shown in **Table S5**. Total RNA of *S. xylosus* and mutant *S. xylosus* was extracted. Then, the equivalent amount of total DNA-free RNA from the last sample was reverse-transcribed using Prim-Script TM RT reagent kit with gDNA Eraser. Ultimately, the real-time PCR reactions were performed for 40 cycles (95 ℃ for 15 s, 60 ℃ for 35 s) after initial 30 s incubation at 95 ℃. The assays were repeated 3 times.

## Statistical analysis

All MIC values were determined in triplicate to ensure reliability. Data on real-time PCR were analyzed (and figures drawn) using GraphPad Prism. DNAMAN and blast was applied to identify the DNA sequence.

# Results And Discussion

**Mutations in ribosomal proteins of tylosin-resistant** S. xylosus

To probe the molecular evolution of tylosin-resistant *S. xylosus*, we sequenced PCR amplified DNA of ribosomal proteins L3, L4 and L22 from *S.xylosus* and tylosin-resistant *S.xylosus* **(Figure S4)**. Sequencing revealed mutations N135G, A137G, S142A and R162K in ribosomal protein L3 at gene locus (*rplC*), S158N and A164E in L4 at locus (*rplD*), and 97KRTSAIN98 insertion in L22 at locus (*rplV*) **(Figure S4)**. The L3 loop F127-P170 is located in the vicinity of PTC, and deletions or mutations in the loop may reshape the drug-binding pocket hindering antibiotic binding of *Staphylococcus aureus* [32]. The mutations of L3 found in our present study are consistent with results of our previous study. Hence, we conclude that mutations N135G, A137G, S142A and R162K in L3 are involved in the molecular evolution of cross resistance. In addition, the L4 W65-Q75 loop is located in the vicinity of the phosphate of ribosomal RNA A2059, which belongs to the multidrug-binding pocket, and mutations in the W65-Q75 loop might affect the conformation of A2059 leading to multi-drug resistance [33]. However, the mutations of L4 found in our present study are not in line with the region mentioned before. In addition, the point mutations, deletions, and insertions in the L22 hairpin loop, which is part of the exit tunnel R80-S108, would confer resistance to erythromycin, synercid and telithromycin in multi-drug resistant *S. aureus* [34, 35]. Hence, it is reasonable that 97KRTSAIN98 insertion in L22 are involved in the molecular evolution of cross resistance.

**Identification of mutant** S. xylosus

Our protein sequence analysis related distinct mutations of ribosomal proteins L3 (*rplC*), L4 (*rplD*) and L22 (*rplV*) to tylosin-resistance of *S. xylosus*. Next, the ribosomal mutant *S. xylosus* were constructed, and the *gfp* gene instead of resistance genes as screening flag was used to find mutant strains [26]. Since, in our study, our aim was to clarify the drug resistant mechanism, and the resistance genes would disturb the results. Then, flow cytometry (FC) was used to detect mutant strains on the basis of the fluorescence of expressed *gfp* gene. Compared with wild-type strain, the screened strains showed strong fluorescence, and fluorescence intensity continually increased along with screening generations **(**Fig. 2A**)**. Furthermore, the screened strains were further identified by PCR amplification and sequencing **(Figure S5)**. As expected, the sequencing results of the amplified fragments were in accord with the introduced mutant sites **(Figure S6)**.

**Determination of mutant** S. xylosus **susceptibility**

Next, we carried out MIC assays to seek which mutant sites were related to molecular evolution mechanism of the tylosin-resistance. The resistance to tylosin increased from 0.5 μg/mL in wild-type *S. xylosus* to 128 μg/mL in L22 (*rplV*) mutant **(**Table 1**)**. We made an additional interesting obsrvation, that

the MIC against florfenicol increased from 0.5 μg/mL in wild-type *S. xylosus* to 2 μg/mL in L22 (*rplV*) mutant (Table 1). In contrast, the resistance to tylosin and florfenicol did not change for L3 (*rplC*) and L4 (*rplD*) mutant compared to wild-type *S.xylosus.*

Table 1
MIC of ribosomal mutant *S. xylosus*

| Strains | Tylosin (ug/mL) | Florenicol (ug/mL) |
|---|---|---|
| *S. xylosus* | 0.5 | 0.5 |
| Tylosin-resistant *S. xylosus* | 128 | 4 |
| L3 (*rplC*) N135G, A137G, S142A and R162K mutant *S.xylosus* | 0.5 | 0.5 |
| L4 (*rplD*) S158N and A164E mutant *S.xylosus* | 0.5 | 0.5 |
| L22 (*rplV*) 97KRTSAIN98 insertion mutant *S.xylosus* | 128 | 2 |

**The structure of tylosin and florfenicol bound to the large ribosomal subunit of S.** xylosus

Crystal structures of ribosomal subunit from *S. xylosus* in the absence or presence of bound antibiotic and *S. xylosus*/antibiotic complex have not been reported yet, making it difficult to understand the structural relationship between *S. xylosus* and the two antibiotics, tylosin and florfenicol. Fortunately, co-crystal structure of tylosin bound to the related 50S ribosomal subunit of *Haloarcula marismortui* has been resolved. This study revealed tylosin bound in a narrow part of the ribosomal peptide exit tunnel at a site that lies between the peptidyl transferase center and the constriction in the tunnel near protein L22 [36]. The crystal structure of the 50S ribosomal subunit complexed with the clinically relevant antibiotics chloramphenicol, a closely related chemical structures to florfenicol, shows that the antibiotic binding site is composed exclusively of segments of 23S ribosomal RNA at the entrance to the peptide exit tunnel or the peptidyl transferase cavity [24]. Based on these studies, we suggest that tylosin and florfenicol contact primarily the peptide exit tunnel or PTC of 23S rRNA of *S. xylosus* and the mycinose moiety of tylosin binds L22.

Here, we used computational methods to construct three-dimensional structure of 23S rRNA and L22 of *S. xylosus* and then dock antibiotics to the structure to elucidate the structural basis of ribosome-antibiotic interactions. We used a fully automatic procedure with SWISS-MODEL [37] to model L22 of *S. xylosus* based a related homologous L22 from *S. aureus* (PDB ID: 4WCE) [38] which shared 96% sequence identity. The homology model of *S. xylosus* L22 share a common overall structure of L22 from other species [36, 38]. It consists of a globular domain with three α-helices and an extended loop with two of three-stranded antiparallel β-sheet forming a β-hairpin, which extends approximately 30 Å from the globular domain (Fig. 3A and 3B). Because present homology modeling of RNA remains challenging [39, 40], a more effective method to build *S. xylosus* 23S rRNA is implemented. We found that the sequence alignment of the 23S rRNA of 50S nucleotides shows 93% identity with only 97 different bases between

*S. xylosus* and *S. aureus* **(Figure S7)**. For the high sequence conservation, we directly mutated these local bases in the crystal structure of *S. aureus* 23S rRNA to build the initial three-dimensional structure for *S. xylosus* 23S rRNA. Then, we combined the homology model of L22 and the mutant 23S rRNA into a new *S. xylosus* model. The interactions between bases and sidechains of amino acids, and those between sidechains of amino acids in this new model were re-calibrated by performing MD simulations which provided a more reasonable *S. xylosus* structure **(**Fig. 3C**)**. The MD trajectory showed that RMSD of 23S rRNA and L22 within 1.4 Å during 5 ns simulation **(Figure S8)**, suggesting that the molecular interactions in this new *S. xylosus* mode were stable.

Then, we extracted the last configuration from the simulation trajectory as a starter to obtain *S. xylosus*-antibiotics complex model. As indicated in Fig. 4, S. *xylosus* ribosomal subunit complexed with tylosin shows that the saccharide branch linked to lactone ring C5 contacts with the PTC and the mycinose linked to C14 that points to the exit tunnel consisting with L22 and domain Ⅴ of 23S rRNA. It was similar to the binding orientation in other ribosome-tylosin complexes elsewhere [41]. The tylosin-binding sites include nucleotides A798 (A748, *E. coli*), A2086 (A2041, *E. coli*), A2090 (A2045, *E. coli*), G2533 (G2508, *E. coli*), U2637 (U2575, *E. coli*) and L22 Gln90, which establish either hydrophobic or hydrogen bond interactions with ligand. In the model of *S. xylosus*-florfenicol, florfenicol was bound at the PTC with the OH- and the NH groups forming hydrogen bonds with A2479 (A2454, *E. coli*) and A2533 (A2508, *E. coli*). Those results clearly illustrate that tylosin is bound at the polypeptide exit tunnel which may inhibit translation by blocking the egress of nascent polypeptides. In contrast, florfenicol binding site is located at the A-site and may block PTC activity by hampering the binding of transfer RNA to the A-site.

# Structural Analysis Of L22 Resistance Mechanism

The resistance to tylosin increased from 0.5 μg/mL in wild-type *S. xylosus* to 128 μg/mL in L22 (*rplV*) mutant, whereas that of florfenicol changed from 0.5μg/mL to 2 μg/mL **(**Table 1**)**. The effect of the mutations identified on the L22 structure was investigated by both molecular modelling and MD simulations. According to the modelled structures, the mutated site of L22 (*rplV*) was located in the β-hairpin of the wildtype L22 **(Figure S9)**. Therefore, it could potentially destroy the hairpin secondary structure. Considering the flexibility of protein which ruled function and controlled activity, we further investigated the structure and motion of wild-type as well as mutant L22 using MD simulations. As shown in Fig. 5A, the L22 protein extended β hairpin remained stable in a folded sheet structure in the wild-type. In contrast, the mutant protein in this region became highly flexible and disordered, supporting mutant-induced β-hairpin disruption in L22 (*rplV*) (Fig. 5B). We used principle component analysis (PCA) [42] to calculate the protein backbone motion in the MD trajectory. This analysis revealed that the mutant insertion residues were unstructured and underwent large changes bracking the β-hairpin formation **(**Fig. 5B**)**. Furthermore, docking study indicated that the tylosin binding site interacted with the mycinose moiety with the L22 β-hairpin. An apparent disruption of the conformation of the extended β-hairpin might directly influence tylosin binding. In addition, this hairpin contributed to the formation of part of the ribosomal tunnel wall for the exit of the nascent peptide **(**Fig. 5C**)** along with 23S rRNA and ribosomal

protein L4. The L22 mutant could change the surface properties or perturb the three-dimensional structure of the tunnel wall. Therefore, it might influence translation by regulating the exit of nascent peptides. Taken together, the L22 (*rplV*) 97KRTSAIN98 insertion mutant has double effects on the tylosin-resistance: (1) Breaking the interaction of the tylosin mycinose moiety with the L22 β-hairpin. (2) Altering the structure of the exit tunnel wall. In contrast, as no direct contact was found between L22 and florfenicol, the resistance most likely occurrs indirectly via perturbation of the exit tunnel wall. This is in agreement with the observation that the MIC of mutant strains against florfenicol did not return to the level of resistant strains.

To further investigate the role of mutations in L3 and L4, we constructed three-dimensional structures of L3 and L3 (*rplC*) mutant, and L4 and L4 (*rplD*) mutant based on homologous structure from *S. aureus* (PDB ID: 4WCE) which shared 90% sequence identity. Comparing these modelled structures, no structural difference between wild-type and mutant are evident **(Figure S10A and B)**. In particular, all of the mutated amino acids in the modeled structures are not adjacent to the tylosin and florfenicol binding pockets and to the exit tunnel of nascent peptide **(Figure S10C)**, indicating that these mutations do not alter the binding of these two antibiotics and disrupt the progression of the nascent peptide.

**Identification of resistant proteins in evolution of tylosin-resistant** S. xylosus **and L22 mutant** S. xylosus **at mRNA level**

Elsewhere it was suggested that antibiotic resistance might not only depend on mutations in ribosomal proteins, but might also be influenced by the interaction network of bacterial proteins [43]. Elsewhere we recently showed that proteins related to stress-response and transcription in the tylosin resistant *S. xylosus* markedly changed at mRNA level [44]. We concluded that during the evolution of tylosin and florfenicol resistant *S.xylosus*, expressionn of the above resistant proteins may change at mRNA level. In order to identify the relationship of the resistant proteins to the evolution of tylosin-resistance in *S. xylosus*, the involved proteins have been probed at the mRNA level. As shown in Fig. 2B, the mRNA level of *rplW* (50S ribosomal protein L23), *aldA* (aldelyde dehydrogenase), *trxA* (thioredoxin), *gros* (chaperonin) gradually increased during the evolution of tylosin-resistance in *S. xylosus* while the mRNA concentration of *ldh* (lactate dehydrogenase) was reduced. These results confirm the influence of the corresponding proteins on the evolution of tylosin-resistance in *S. xylosus*.

To explore the relationship of mutations in the ribosomal proteins for the development of tylosin-resistance in *S. xylosus* further, we determined the mRNA level of resistant proteins in the L22 mutant of *S. xylosus*. The results of these investigations, summarized in Fig. 2C, show that the mRNA level of the resistant proteins, including thioredoxin (*trxA*), 50S ribosomal protein L23 (*rplW*), aldelyde dehydrgenase (*aldA-1*), chaperonin (*gros*), L- lactic dehydrogenase (*ldh*) and chloramphenicol resistant protein (*cl*) in the L22 mutant strain changed significantly, demonstrating that the resistant proteins were regulated by ribosomal protein L22.

In summary, our study strongly suggests that tylosin-resistant *S.xylosus* cross-resistance to florfenicol originates from a distinct mutation (*rplV*) in the sequence of the ribosomal protein L22 which contains

97KRTSAIN98 insertion. Computational analysis fostered this proposition revealing atomic details for the action of the two antibiotics (Fig. 6): Tylosin is bound to the ribosomal polypeptide exit tunnel adjacent to the PTC, whereas florfenicol is bound to the PTC blocking A-site. The evolution of increasing resistance of *S.xylosus* against tylosin and florfenicol is related to interaction network of bacterial proteins. Proteins including thioredoxin (*trxA*), 50S ribosomal protein L23 (*rplW*), aldelyde dehydrgenase (*aldA-1*), chaperonin (*gros*), L- lactic dehydrogenase (*ldh*) and chloramphenicol resistant protein (*cl*) are regulated by ribosomal L22 which indicates the importance of regulation of the ribosomal protein network in cross resistance. Our work provides insightful views into the molecular mechanism of *S. xylosus* resistance which could be useful for the development of the next generation antibiotics.

# Declarations

### Ethics approval and consent to participate

Not applicable

### Consent for publication

Not applicable

### Availability of data and material

The authors confirm that the data supporting the findings of this study are available within the article and its supplementary materials.

### Competing interests

All authors declare no competing interests.


### Funding

We appreciate financial support by the earmarked funding for China Agriculture Research System-35 and National Key Research and Development Program of China under Grant number 2018YFD0500300 and National Nature Science Foundation of China under Grant number 31772787. The work of Shuguang Yuan was supported by funding from Chinese Academy of Sciences, the Shenzhen Institutes of Advanced Technology, CAS, Shenzhen government under Grant number JCYJ20200109114818703 as well as that from Guangdong province under Grant number 2019QN01Y306. The work of Horst Vogel was supported by the Shenzhen government under Grant number 2020FSB0003 as well as Chinese Academy of Sciences. The work of Xin Liu was supported by the Science and Technology Foundation of Guizhou Province under Grant number Qianke He Foundation -ZK[2021]General 083 . We appreciated the supports of computer resources from the Polish National Supercomputer Center.


### Authors' contributions

Shuguang Yuan, Horst Vogel & Yanhua Li lead the whole project. Xin Liu, Yonghui Zhou, Mo Chen, Qianwei Qu, Ruixiang Che and Lu Li performed the biochemistry testing. Shu Li & Wenqiang Cui performed molecular modelling as well as molecular simulations. Xin Liu, Shu Li & Shuguang Yuan prepared figures. All authors read and revised the manuscript.

**Acknowledgements**

We also thank Prof. Rui Zhou (Huazhong Agricultural University) for the help with pBT2.

**Authors' information**

Xin Liu[1, 2, #], Shu Li[3, #], Wenqiang Cui[3], Yonghui Zhou[2], Mo Chen[1], Qianwei Qu[1], Ruixiang Che[4], Lu Li[5], Horst Vogel[3, 6*], Shuguang Yuan[3, *], Yanhua Li[1, *]

1 College of Veterinary Medicine, Northeast Agricultural University, Harbin, Heilongjiang 150030, China

2 College of Basic Medicine, Guizhou University Of Traditional Chinese Medicine, Guiyang, Guizhou 550025, China

3 The Research Center for Computer-aided Drug Discovery, Shenzhen Institutes of Advanced Technology, Chinese Academy of Sciences, Shenzhen 518055, China

4 College of Animal Science and Veterinary Medicine, Heilongjiang Bayi Agricultural University, Daqing 163319, China

5 College of Life Sciences, Northeast Agricultural University, Harbin, Heilongjiang 150030, China

6 Institute of Chemical Science and Engineering (ISIC), Ecole Polytechnique Fédérale de Lausanne (EPFL), Lausanne, Switzerland.

[#] These authors contributed equally to this work.

*** Corresponding authors:**

Email: horst.vogel@epfl.ch (Horst Vogel), shuguang.yuan@siat.ac.cn (Shuguang Yuan), liyanhua@neau.edu.cn (Yanhua Li).

# References

1. Wilson DN, Hauryliuk V, Atkinson GC, O'Neill AJ (2020) Target protection as a key antibiotic resistance mechanism. Nat Rev Microbiol 18:1–12
2. Fan L, Xiao HP (2018) [The thinking and challenge from the drug-resistant tuberculosis guidelines by World Health Organization], *Zhonghua jie he he hu xi za zhi = Zhonghua jiehe he huxi zazhi = Chinese*. journal of tuberculosis respiratory diseases 41:3–5

3. Tangcharoensathien V, Sattayawutthipong W, Kanjanapimai S, Kanpravidth W, Brown R, Sommanustweechai A (2017) Antimicrobial resistance: from global agenda to national strategic plan, Thailand. Bull World Health Organ 95:599–603
4. Charmpi C, Veken DVD, Reckem EV, Vuyst LD, Leroy F (2020) Raw meat quality and salt levels affect the bacterial species diversity and community dynamics during the fermentation of pork mince. Food Microbiol 89:103434
5. Visscher AD, Piepers S, Haesebrouck F, Supre K, Vliegher SD (2017) Coagulase-negative Staphylococcus species in bulk milk: Prevalence, distribution, and associated subgroup- and species-specific risk factors. J Dairy Sci 100:629–642
6. Wang D, Zhao L, Su R, Jin Y (2019) Effects of different starter culture combinations on microbial counts and physico-chemical properties in dry fermented mutton sausages. *Food Science & Nutrition*
7. Rissi DR, Elsmo EJ, Sanchez S (2015) Cystitis and peritonitis caused by Staphylococcus xylosus infection in a calf, *Brazilian Journal of Veterinary Pathology*
8. Giordano N, Corallo C, Miracco C, Papakostas P, Montella A, Figura N, Nuti R (2016) Erythema nodosum associated with Staphylococcus xylosus septicemia. J Microbiol Immunol Infect 49:134–137
9. Jabbar H, Al-Mathkhury F, Flaih MT, Khalil H (2014) Histopathological effects of S. xylosus peptidoglycan in comparison to E. coli lipopolysaccharide in the urinary tract of mice. Turk J Med Sci 42:1278–1285
10. Seif S, El-Rehewy M, Ghazaly M, Abd-Elhamid M (2020) Biofilm Formation by Blood Stream Staphylococcal Isolates from Febrile Pediatric Cancer Patients at South Egypt Cancer Institute
11. Miracco C, Camillo, Claudio, Papakostas, Panagiotis, Giordano, Nicola, Montella, and Antonio. (2016) Erythema nodosum associated with Staphylococcus xylosus septicemia, *Journal of microbiology, immunology, and infection: Wei mian yu gan ran za zhi*
12. Aqeel S, Omran, Azhar, Noory, and Hussein (2019) Molecular investigation of Mecgene Among coagulase negative Staphylococcus isolated from different cases, *Journal of Physics: Conference Series 1234*, 12074–12074
13. Wang J, Qu Q, Liu X, Cui W, Li Y (2020) 1-Hydroxyanthraquinone exhibited antibacterial activity by regulating glutamine synthetase of Staphylococcus xylosus as a virulence factor. Biomedicine pharmacotherapy = Biomedecine pharmacotherapie 123:109779
14. Macfadyen AC, Leroy S, Harrison EM, Parkhill J, Paterson GK (2019) Staphylococcus pseudoxylosus sp. nov., isolated from bovine mastitis, *International Journal of Systematic and Evolutionary Microbiology 69*
15. Klibi A, Jouini A, Andolsi RBE, Kmiha S, Maaroufi A (2019) Epidemiology of β -Lactamase-Producing Staphylococci and Gram Negative Bacteria as Cause of Clinical Bovine Mastitis in Tunisia, *BioMed Research International 2019*, 1–9
16. Ndahetuye JB, Persson Y, Nyman AK, Tukei M, Ongol MP, Bge R (2019) Aetiology and prevalence of subclinical mastitis in dairy herds in peri-urban areas of Kigali in Rwanda, *Springer Open Choice 51*

17. De Almeida CC, Pizauro LJL, Soltes GA, Slavic D, de Ávila FA, Pizauro JM, Macinnes JI (2018) Some coagulase negative Staphylococcus spp. isolated from buffalo can be misidentified as Staphylococcus aureus by phenotypic and Sa442 PCR methods, *Bmc Research Notes 11*
18. Russo M, Invernizzi A, Gobbi A, Radaelli E (2013) Diffuse Scaling Dermatitis in an Athymic Nude Mouse. Vet Pathol 50:722–726
19. Baqer BAAA, Mahdi LH (2019) Biofilm Formation and Antibiotic Resistance of Coagulase-Negative Staphylococci Isolated from Lactating Women with Mastitis in Baghdad, Iraq. Indian Journal of Public Health Research Development 10:2175
20. Claudia G, Raspanti, Cesar C, Bonetto, Claudina V, Matías, and S (2016) Prevalence and antibiotic susceptibility of coagulase-negative Staphylococcus species from bovine subclinical mastitis in dairy herds in the central region of Argentina - ScienceDirect. Revista Argentina de Microbiología 48:50–56
21. Dean Z (2019) Antibiotic interactions, collateral sensitivity, and the evolution of multidrug resistance in E. faecalis
22. Sebastian K, John, and Woolford (2018) Ribosome assembly coming into focus, *Nature Reviews Molecular Cell Biology*
23. Hansen JL, Moore PB, Steitz TA (2020) *Structures of Five Antibiotics Bound at the Peptidyl Transferase Center of the Large Ribosomal Subunit*
24. Vázquez-Laslop N, Mankin AS (2018) How Macrolide Antibiotics Work, *Trends in Biochemical Sciences*
25. Marks J, Kannan K, Roncase EJ, Klepacki D, Kefı A, Orelle C, Vazquez-Laslop N, Mankin AS (2016) Context-specific inhibition of translation by ribosomal antibiotics targeting the peptidyl transferase center. Proc Natl Acad Sci USA 113:12150–12155
26. Zhou YH, Xu CG, Yang YB, Xing XX, Liu X, Qu QW, Ding WY, Bello-Onaghise G, Li YH (2018) Histidine Metabolism and IGPD Play a Key Role in Cefquinome Inhibiting Biofilm Formation of Staphylococcus xylosus, *Front Microbiol 9*, 665-
27. Brückner R (2010) Gene replacement in Staphylococcus carnosus and Staphylococcus xylosus. Fems Microbiology Letters 151:1–8
28. Xu CG, Yang YB, Zhou YH, Hao MQ, Ren YZ, Wang XT, Chen JQ, Muhammad I, Wang S, Liu D (2017) Comparative Proteomic Analysis Provides insight into the Key Proteins as Possible Targets Involved in Aspirin Inhibiting Biofilm Formation of Staphylococcus xylosus. Front Pharmacol 8:543-
29. Abraham MJ, Murtola T, Schulz R, Páll S, Lindahl E (2015) GROMACS: High performance molecular simulations through multi-level parallelism from laptops to supercomputers, *Softwarex 1–2*, 19–25
30. Lindorff-Larsen K, Piana S, Palmo K, Maragakis P, Klepeis JL, Dror RO, Shaw DE (2010) Improved side-chain torsion potentials for the Amber ff99SB protein force field, *Proteins 78*, 1950–1958
31. Friesner RA, Murphy RB, Repasky MP, Frye LL, Greenwood JR, Halgren TA, Sanschagrin PC, Mainz DT (2006) Extra precision glide: docking and scoring incorporating a model of hydrophobic enclosure for protein-ligand complexes, *Journal of medicinal chemistry 49*, 6177–6196

32. Zohar E, Donna M, Miri K, Itai W, Susanne P, Ella Z, Haim R, Anat B, Ada Y (2015) Structural insights into species-specific features of the ribosome from the pathogen Staphylococcus aureus. Proc Natl Acad Sci USA 112:5805–5814
33. F S, R, Z., J, H., A, B., A, T., R, A., A, Y., and F F (2001) Structural basis for the interaction of antibiotics with the peptidyl transferase centre in eubacteria. Nature 413:814–821
34. Gentry D, Holmes D (2008) Selection for high-level telithromycin resistance in Staphylococcus aureus yields mutants resulting from an rplB-to-rplV gene conversion-like event. Antimicrobial Agents Chemotherapy 52:1156–1158
35. Brigitte M, Annie C, Bülent B, Bruno F, Virginie Z, Sylvie DM, Celine F, Roland L (2002) Resistance to quinupristin-dalfopristin due to mutation of L22 ribosomal protein in Staphylococcus aureus. Antimicrobial Agents Chemotherapy 46:2200
36. Hansen JL, Ippolito JA, Ban N, Nissen P, Moore PB, Steitz TA (2002) The structures of four macrolide antibiotics bound to the large ribosomal subunit. Mol Cell 10:117–128
37. Waterhouse A, Bertoni M, Bienert S, Studer G, Tauriello G, Gumienny R, Heer FT, de Beer TAP, Rempfer C, Bordoli L, Lepore R, Schwede T (2018) SWISS-MODEL: homology modelling of protein structures and complexes, *Nucleic acids research 46*, W296-W303
38. Eyal Z, Matzov D, Krupkin M, Wekselman I, Paukner S, Zimmerman E, Rozenberg H, Bashan A, Yonath A (2015) Structural insights into species-specific features of the ribosome from the pathogen Staphylococcus aureus. Proc Natl Acad Sci USA 112:E5805–E5814
39. Somarowthu S (2016) Progress and Current Challenges in Modeling Large RNAs. Journal of molecular biology 428:736–747
40. Sponer J, Bussi G, Krepl M, Banas P, Bottaro S, Cunha RA, Gil-Ley A, Pinamonti G, Poblete S, Jurecka P, Walter NG, Otyepka M (2018) RNA Structural Dynamics As Captured by Molecular Simulations: A Comprehensive Overview, *Chemical reviews 118*, 4177–4338
41. Hansen JL, Ippolito JA, Ban N, Nissen P, Steitz TA (2002) The Structures of Four Macrolide Antibiotics Bound to the Large Ribosomal Subunit. Mol Cell 10:117–128
42. Bakan A, Meireles LM, Bahar I (2011) ProDy: protein dynamics inferred from theory and experiments, *Bioinformatics 27*, 1575–1577
43. Kohanski MA, Dwyer DJ, Collins JJ (2010) How antibiotics kill bacteria: from targets to networks. Nat Rev Microbiol 8:423–435
44. Liu X, Wang J, Chen M, Che R, Li Y (2019) Comparative proteomic analysis reveals drug resistance of Staphylococcus xylosus ATCC700404 under tylosin stress, *BMC Veterinary Research 15*

# Figures

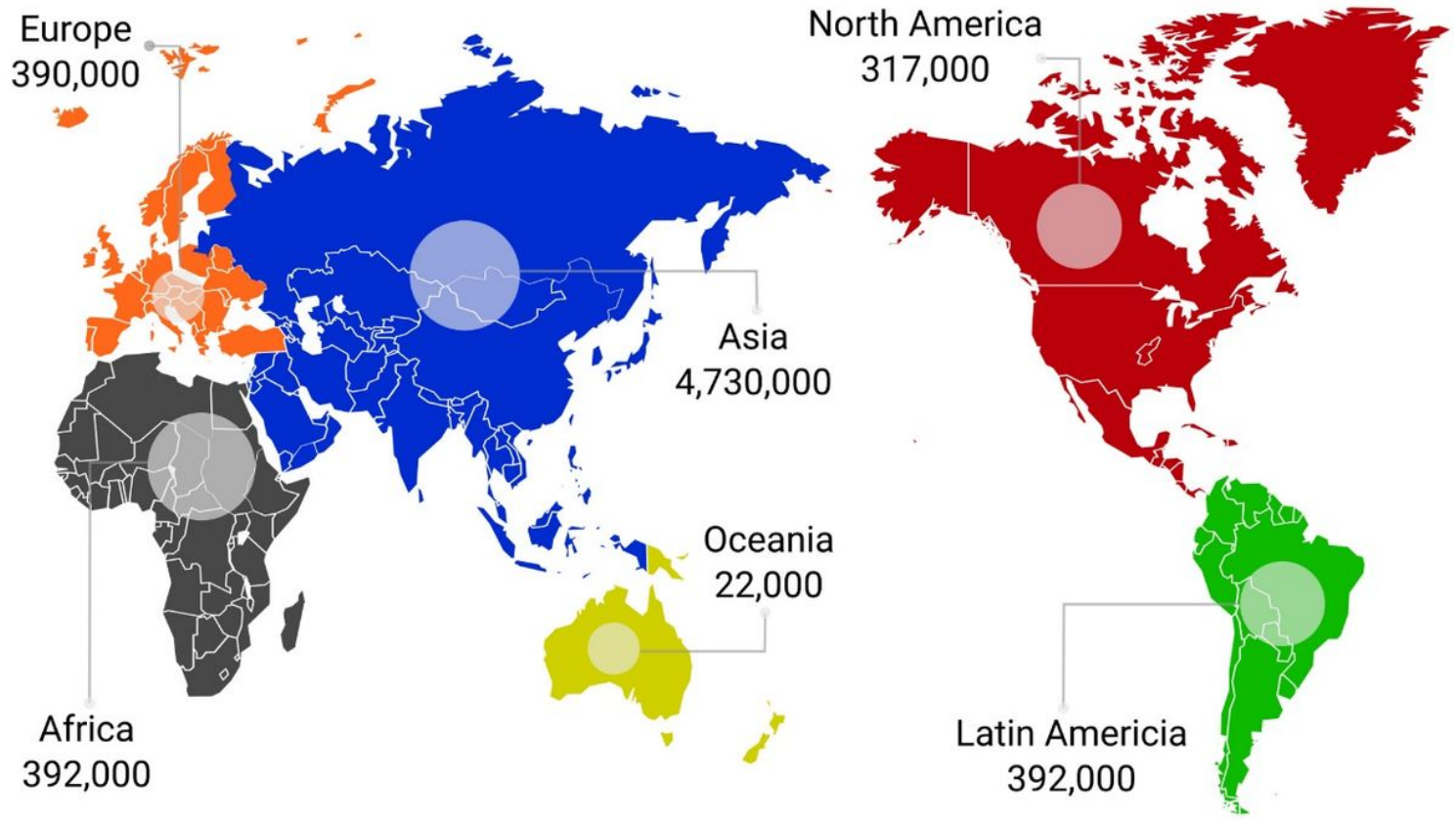


**Figure 1**

The annual global death attribute to antibiotics resistance by 2050. Note: The designations employed and the presentation of the material on this map do not imply the expression of any opinion whatsoever on the part of Research Square concerning the legal status of any country, territory, city or area or of its authorities, or concerning the delimitation of its frontiers or boundaries. This map has been provided by the authors.

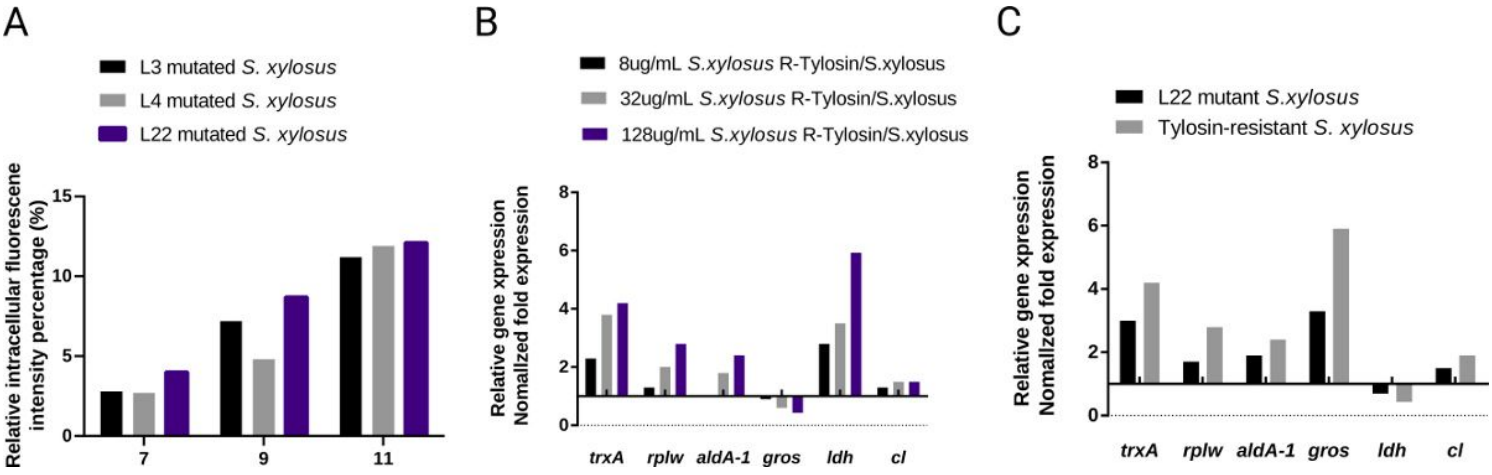


**Figure 2**

(A) Flow cytometry was used to measure the florescence of GFP in mutated S.xylosus, after 7, 9 and 11 generations. (B) Thioredoxin (trxA), 50S ribosomal protein L23 (rplW), aldelyde dehydrgenase (aldA-1),

chaperonin (gros), L- lactic dehydrogenase (ldh) and chloramphenicol resistant protein (cl). (C) Changes of resistant proteins at mRNA level of L22 (rplV) mutant S. xylosus, including thioredoxin (trxA), 50S ribosomal protein L23 (rplW), aldelyde dehydrgenase (aldA-1), chaperonin (gros), L- lactic dehydrogenase (ldh) and chloramphenicol resistant protein (cl).

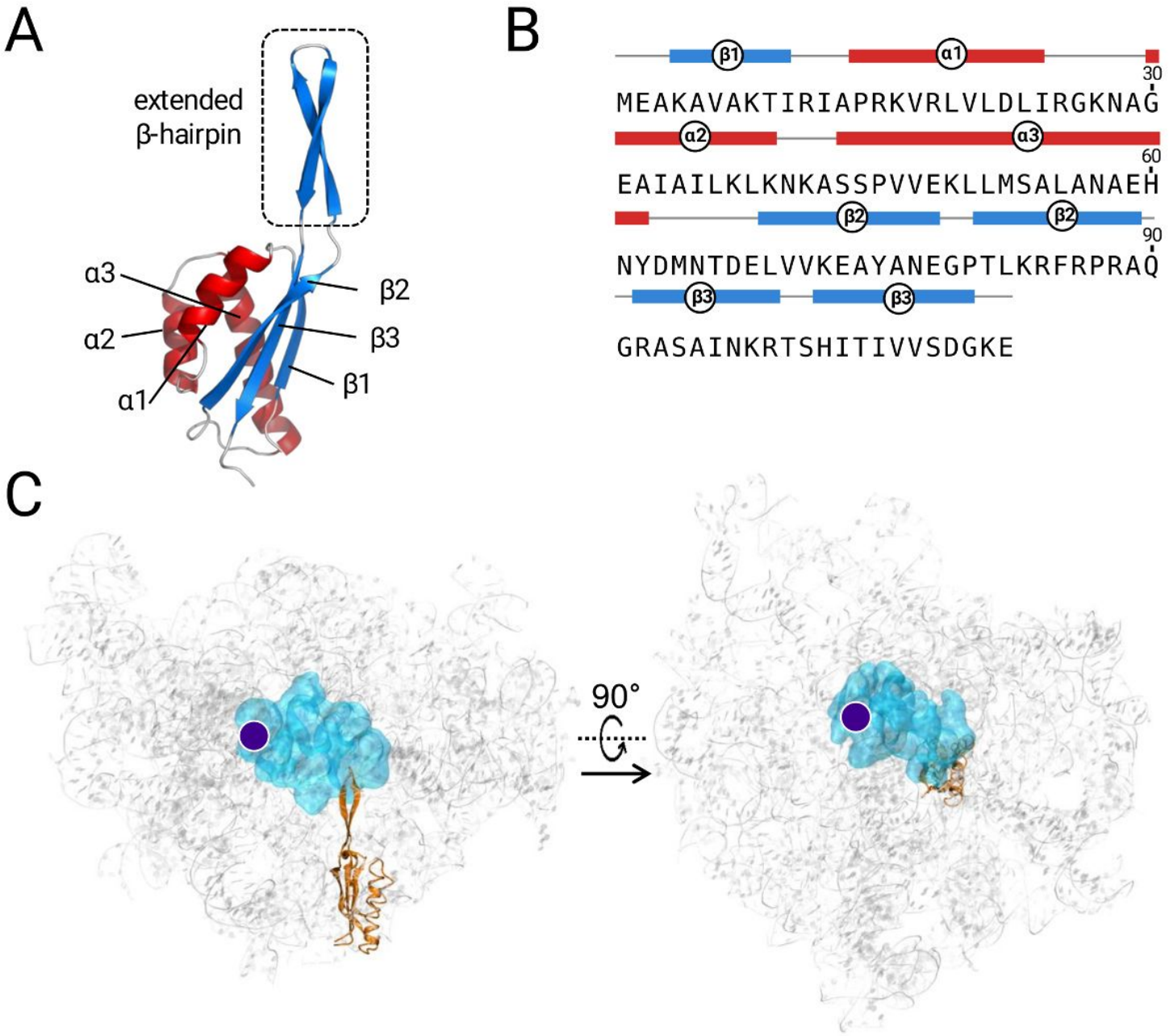


## Figure 3

(A) 3D model of S. xylosus L22. The overall structure consists of three α-helices and three β-strands. The encircled box indicates the location of β-hairpin. (B) The amino acid sequence of L22 together with distribution of particular secondary structures. (C) The overall structure of S. xylosus ribosomal subunit. The 23S rRNA is shown in gray, the L22 is shown in orange, the antibiotic binding site is shown in cyan, whereas the PTC location is marked as a purple dot.

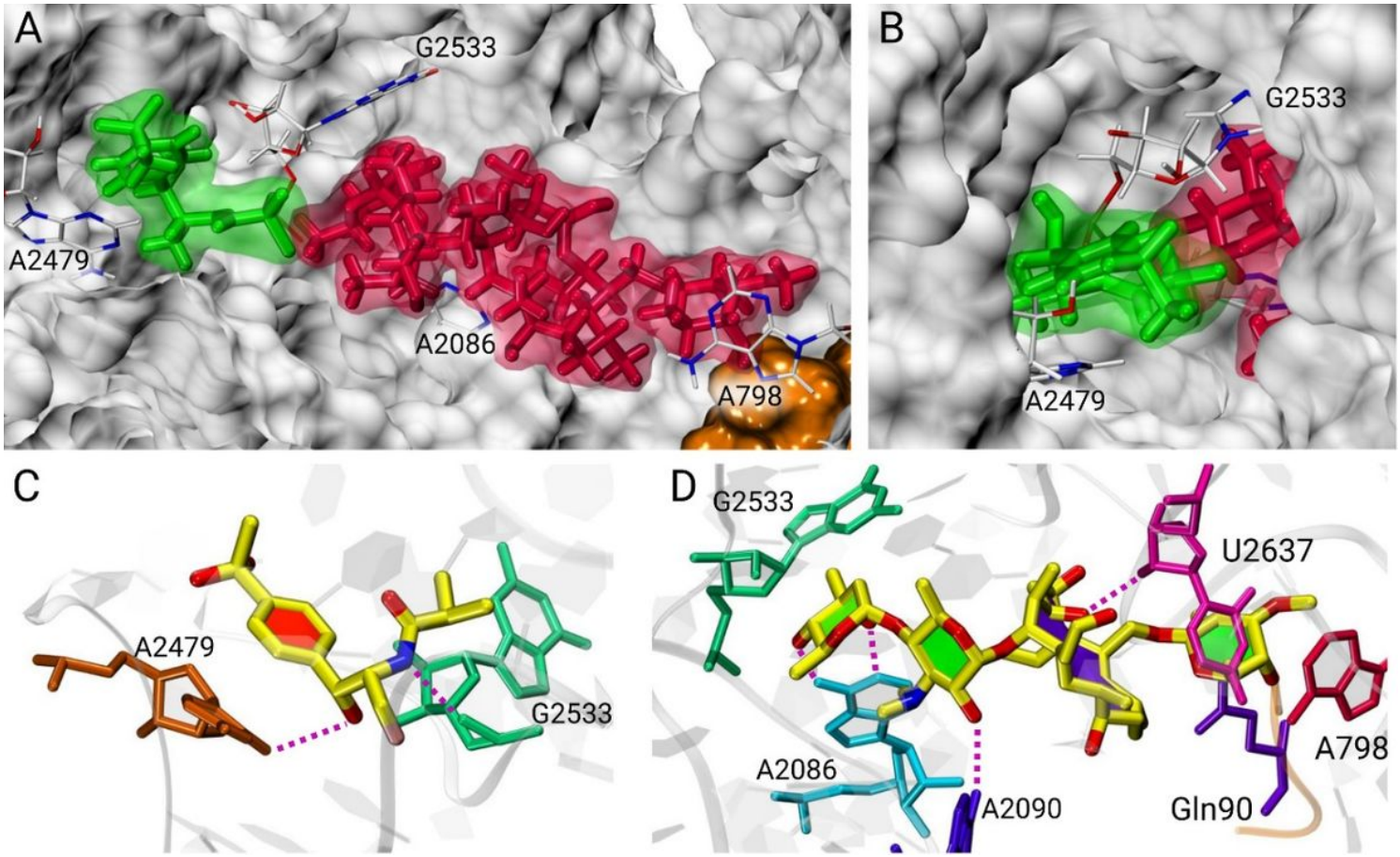


**Figure 4**

A model of antibiotics in complex with the S. xylosus Ribosome. (A) Superposition of the binding locations of tylosin (red) and florfenicol (green). Surface representation of the structure of 23S rRNA (cyan) and that of L22 (orange). Tylosin binds to the peptide exit tunnel, whereas florfenicol is above the exit tunnel of PTC peptide (B). The hydrogen bond interactions (purple dash) of florfenicol (C) and tylosin (D) with 23S rRNA in the ribosome.

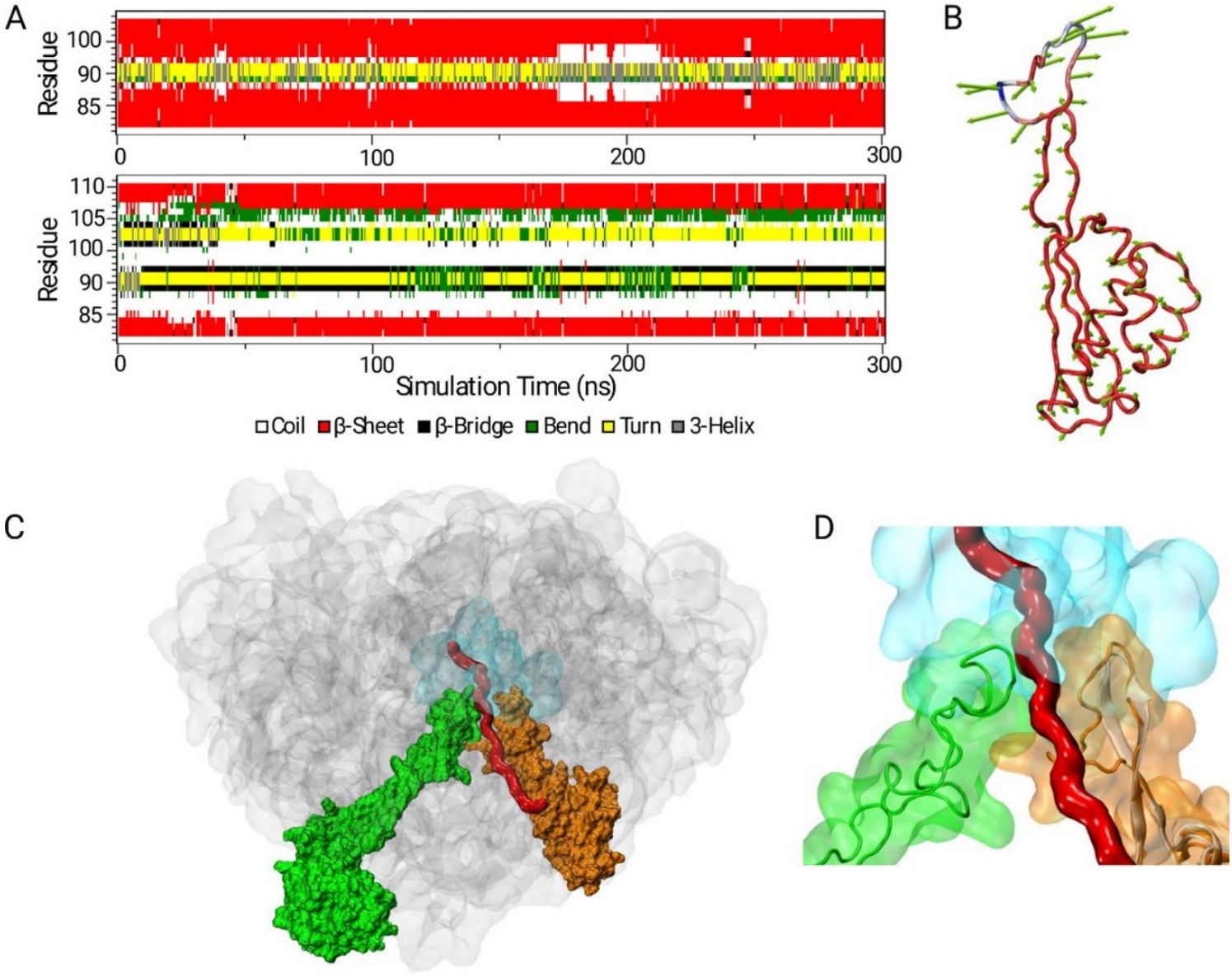


## Figure 5

L22 resistance mechanism. (A) Secondary structure changes of the L22 β-hairpin during MD simulations in the wild type (upper panel) and 97KRTSAIN98 insertion mutant (lower panel). (B) Intrinsic mobility of the L22 mutant calculated from PCA analysis. The lengths of the green vectors scale with the domain-motions. (C, D) Structure of the nascent polypeptide in the exit tunnel. The model of the nascent polypeptide chain is shown in red. The structure of ribosome shown comprises the 23S rRNA and the homology model of L4 and L22 mutant. The 23S rRNA is shown in gray, the antibiotic binding site in cyan, L4 in green and L22 mutant in orange. The wild type L22 is represented as a white cartoon (D).

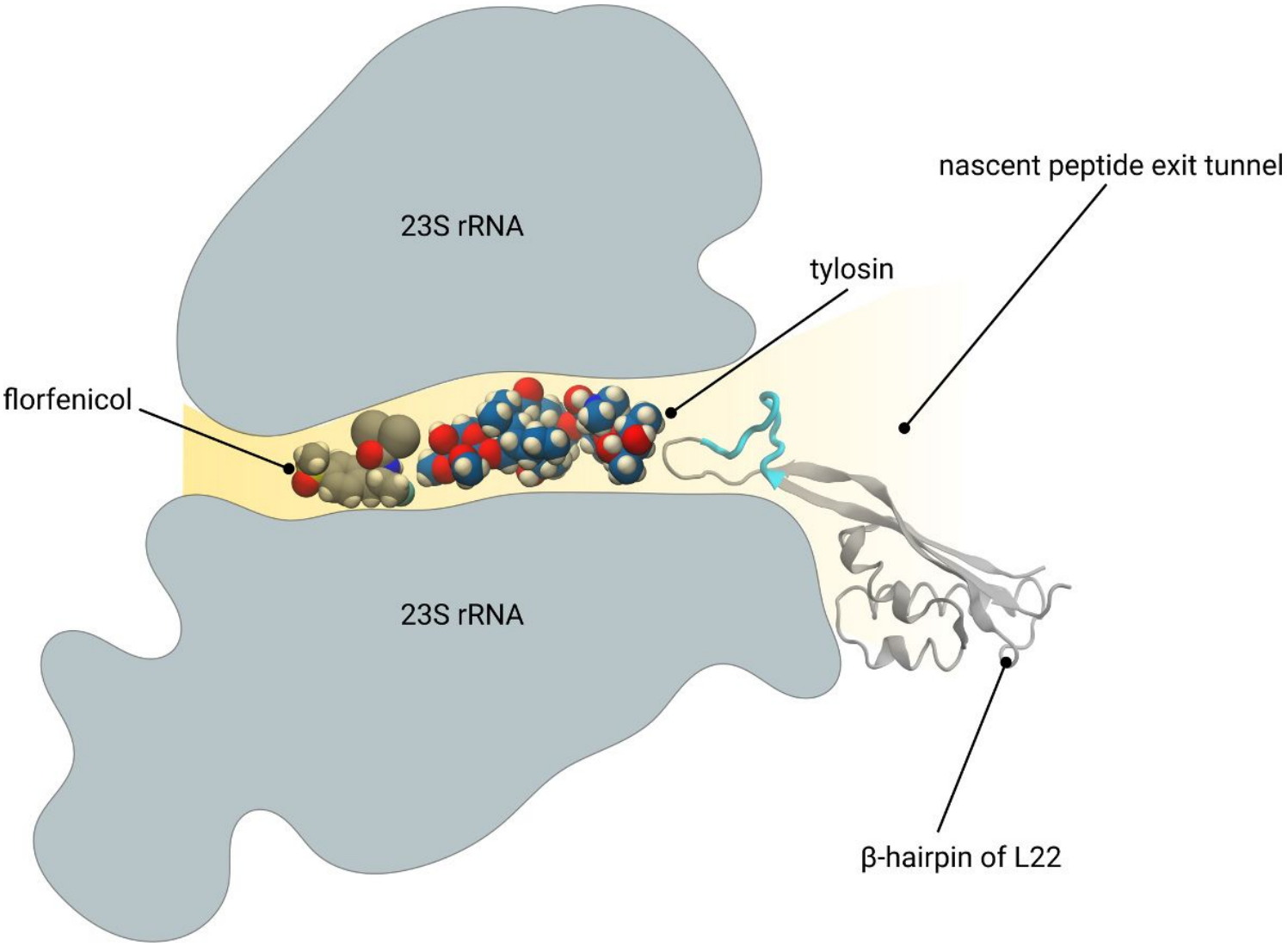


**Figure 6**

The drug-resistance mechanism of tylosin and florfenicol. Florfenicol (gray and red spheres) binds to deep narrow pocket of nascent peptide exit tunnel which is far away from β-hairpin of L22. A loop (in cyan) inserted into the β-hairpin of L22 has limited influence on the drug-resistance of florfenicol. Tylosin (blue and red spheres), which is much larger than florfenicol, binds to the entrance of nascent peptide exit tunnel. It closes to into the β-hairpin of L22. The insertion of additional amino acid (in cyan) shows great impact on the drug-resistance of tylosin.

## Supplementary Files

This is a list of supplementary files associated with this preprint. Click to download.

- SI.docx